Mutational and structural analyses of the regulatory protein B of soluble methane monooxygenase from *Methylococcus capsulatus* (Bath)

Hans Brandstetter[1,2]*, Douglas A Whittington[1], Stephen J Lippard[1] and Christin A Frederick[2]

Background: The soluble methane monooxygenase (sMMO) system in methanotrophic bacteria uses three protein components to catalyze the selective oxidation of methane to methanol. The coupling protein B (MMOB) both activates the carboxylate-bridged diiron center in the hydroxylase (MMOH) for substrate oxidation and couples the reaction to electron transfer from NADH through the sMMO reductase. Although the X-ray structure of the hydroxylase is known, little structural information is available regarding protein B.

Results: Wild-type protein B from *Methylococcus capsulatus* (Bath) is very susceptible to degradation. The triple mutant protein B, Gly10→Ala, Gly13→Gln, Gly16→Ala is resistant to degradation. Analyzing wild-type and mutant forms of protein B using size exclusion chromatography and circular dichroism spectroscopy suggests that the amino terminus of MMOB (Ser1–Ala25) is responsible for the proteolytic sensitivity and unusual mobility of the protein. We used the stable triple glycine protein B mutant to generate an affinity column for the hydroxylase and investigated the interaction between MMOH and MMOB. These results suggest the interaction is dominated by hydrophobic contacts.

Conclusions: A structural model is presented for protein B that explains both its proclivity for degradation and its anomalous behavior during size exclusion chromatography. The model is consistent with previously published biophysical data, including the NMR structure of the phenol hydroxylase regulatory protein P2. Furthermore, this model allows for detailed and testable predictions about the structure of protein B and the role of proposed recognition sites for the hydroxylase.

Addresses: [1]Department of Chemistry, Massachusetts Institute of Technology, Cambridge MA 02139, USA. [2]Department of Biological Chemistry and Molecular Pharmacology, Harvard Medical School and Dana Farber Cancer Institute, Boston MA 02115, USA.

*Present address: Department of Structure Research, Max-Planck-Institute for Biochemistry, D-82125 Martinsried, Germany.

Correspondence: Stephen J Lippard and Christin A Frederick
E-mail: lippard@lippard.mit.edu
caf@red.dfci.harvard.edu

Key words: circular dichroism spectroscopy, glycine hinge, hydroxylase, secondary structure prediction, size exclusion chromatography

Received: **3 March 1999**
Revisions requested: **25 March 1999**
Revisions received: **14 April 1999**
Accepted: **16 April 1999**

Published: **15 June 1999**

Chemistry & Biology July 1999, 6:441–449
http://biomednet.com/elecref/1074552100600441

 ISSN 1074-5521

Introduction

The soluble methane monooxygenase (sMMO) system of methanotrophic bacteria consists of three component proteins that catalyze the conversion of methane to methanol at ambient temperature and pressure (equation 1):

$$CH_4 + O_2 + NADH + H^+ \rightarrow CH_3OH + H_2O + NAD^+ \quad (1)$$

sMMO is of interest for several reasons. First, it could provide a cost-effective way to produce methanol (to be used as an energy source) from the plentiful natural reservoirs of methane gas [1]. Second, methanotrophic bacteria are valuable for bioremediation of the environment [2,3]. This function takes advantage of the broad range of substrates that can be oxidized by sMMO [4,5]. In addition, the flux of methane released naturally by methanogenic bacteria is efficiently controlled by methanotrophs that prevent much of it from reaching the atmosphere [6]. Finally, attention has focused on the catalytic mechanism of the sMMO protein system because of its ability to activate C-H bonds, as well as its structural relationship to ribonucleotide reductase R2 [7] and other nonheme diiron proteins [8].

The sMMO hydroxylase (MMOH) is a homodimer ($\alpha_2\beta_2\gamma_2$, 251 kDa) that contains a catalytic diiron center in the four-helix bundles of its α subunits [9]. Upon addition of NADH, the sMMO reductase component (MMOR, 38.6 kDa) reduces the diiron(III) hydroxylase in two coupled electron-transfer steps forming the diiron(II) enzyme. The coupling protein B (MMOB, 15.9 kDa) and MMOR tune the redox potential of the diiron center to prevent formation of the functionally inactive mixed-valent Fe(II)Fe(III) species [10]. Moreover, in the *Methylococcus capsulatus* (Bath) system, only in the presence of protein B is the fully reduced MMOH able to hydroxylate alkyl substrates with dioxygen, after which it returns to the resting diiron(III) oxidation state [11]. The intimate association between protein B and the hydroxylase is reflected in the sMMO operon, where the gene encoding MMOB is inserted into the MMOH gene cluster. Despite

its central role in the sMMO system, there is little structural information available about protein B, partly because of its intrinsic instability [12,13]. Recently, the structure of a functionally related protein P2 was determined by using nuclear magnetic resonance (NMR) spectroscopy [14]. The P2 polypeptide is required for activity of the multicomponent enzyme phenol hydroxylase, and the P2 gene is similarly integrated into the three genes that code for the phenol hydroxylase subunits [15].

In the present study, engineered MMOB mutants were used to characterize further the instability of the wild-type protein. Although Gly13 is the primary cleavage site, altering this residue alone does not make the protein significantly more stable [13]. Instead, resistance to degradation was conferred on the protein by mutating three glycine residues near the amino terminus of the polypeptide. We also present data using point and truncation mutants of MMOB that directly link the amino-terminal polypeptide Ser1–Ala25 to the anomalous mobility of the protein on size exclusion chromatography. This result has significant implications for a recent report claiming that MMOB from *Methylocystis* sp. strain M is a dimer, based on its behavior during size exclusion chromatography [16]. MMOB binding to the hydroxylase was also strengthened by high salt, suggesting a predominantly hydrophobic interaction between the two proteins. Finally, we present a model for the structure of MMOB that integrates the NMR results on the related P2 protein of phenol hydroxylase with secondary structure predictions; our model is consistent with all available experimental data on MMOB.

Results and discussion

The G10A-G13Q-G16A MMOB mutant protein resists proteolytic degradation

During preparation of MMOB from *M. capsulatus* (Bath), we and others have observed a prominent double band on 15% sodium dodecyl sulfate polyacrylamide gel electrophoresis (SDS–PAGE), corresponding to the full-length protein and a degradation product [12,13]. By amino-terminal sequencing, we determined the major scissile bond to be Met12–Gly13 (Table 1), a result confirmed by mass spectrometry (Table 2). In addition, amino-terminal sequencing revealed the presence of a minor isoform starting with Gly16 (Table 1). These degradation products were observed for protein obtained either from native *M. capsulatus* (Bath) cells or, by recombinant means, from *Escherichia coli*, suggesting proteolysis with glycine as the preferred amino acid after the cleavage site, the so-called P1′ position [17]. Analysis of the *M. capsulatus* (Bath) MMOB sequence identified a cluster of three glycine residues, two of which (Gly10 and Gly16) are conserved in the *Methylosinus trichosporium* OB3b and *Methylocystis* sp. strain M systems (Figure 1) [18]. We therefore tested the effect of these three glycine sites on protein stability using site-directed mutagenesis.

Table 1

Three amino termini identified by sequencing of wild-type protein B from *M. capsulatus* (Bath).

AA1	#	AA2	#	AA3	#	AA4	#	AA5	#
S	1	V	2	N	3	S	4	N	5
G*	13	L	14	K	15	G	16	K	17
G	16	K	17	D	18	F	19	n.d.†	

AA, amino acid (using single-letter amino-acid code). #, Residue position (protein B sequence assignment, cf. Figure 1). *The amino terminus at Gly13 is consistent with [13]. †No amino acid could be unambiguously determined, because this species was less than 5% of the total protein content.

The single-site mutant Gly13→Gln (G13Q) replaces the P1′ residue of the major cleavage site with the corresponding amino acid in the *M. trichosporium* OB3b protein, for which no degradation has been reported in the literature. A similar mutant was described previously [13]. In addition, we examined the triple mutant G10A-G13Q-G16A. Both constructs carry an amino-terminal His_6-tag provided by the pET-15b vector (Novagen), which can be proteolytically cleaved using thrombin. This feature facilitated detection of amino-terminal degradation by affinity chromatography on a Ni^{2+} column. The relative stabilities of the proteins were judged under identical storage conditions (10 mM Tris pH 7.5, 50 mM NaCl, 1 mM DTT, 1 mM EDTA, 4°C). Both wild-type MMOB from *M. capsulatus* (Bath) and the single glycine mutant G13Q began to degrade within days to weeks, as analyzed by SDS–PAGE and Ni^{2+} binding. To a first approximation, this result is consistent with published data that report a 1.2-fold stabilization of the G13Q mutant relative to wild-type protein [13]. The published mutant protein differs from our construct only in the leading amino-terminal amino acids, which originate from the fusion vector into which the published construct was cloned. The presence or absence of the amino-terminal His_6-tag did not affect protein stability.

By contrast, the triple glycine mutant G10A-G13Q-G16A completely resisted proteolysis at 4°C. The homogeneity of this mutant was demonstrated by 15% SDS–PAGE and Ni^{2+} affinity binding for the tagged protein. The stability of this protein is not due to the amino-terminal His_6-tag because, after its removal by thrombin cleavage, there was also no evidence for degradation determined using

Table 2

Mass spectral data to confirm cleavage of wild-type protein B at Met12–Gly13.

Protein species	Calculated mass	Observed mass
S1–A140	15,853 Da	15,851 Da
G13–A140	14,629 Da	14,630 Da*

*These data are consistent with [13].

Figure 1

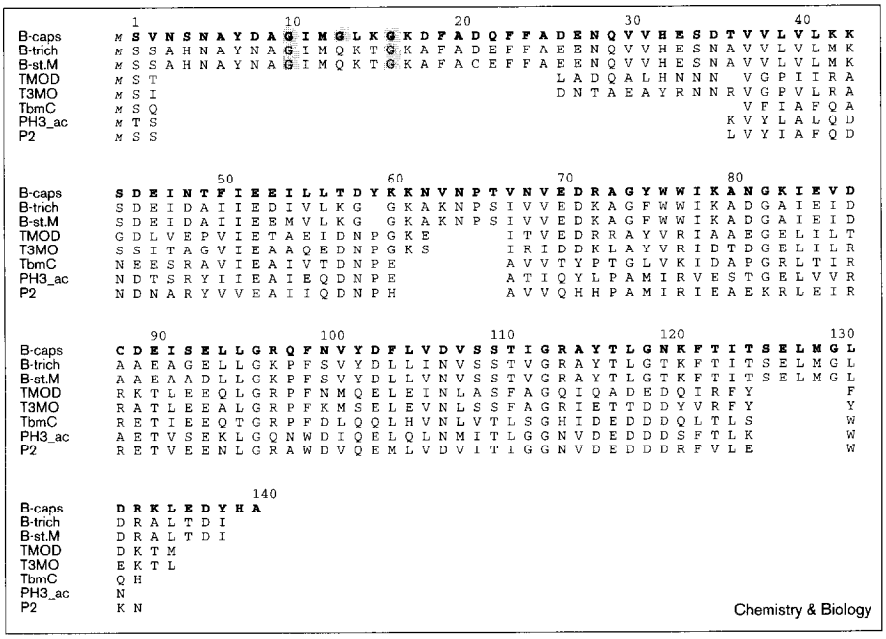

Sequence alignment of related hydroxylase cofactor proteins. The MMOB protein is, according to Tables 1 and 2, completely post-translationally processed and a start methionine is not present in the mature protein. Considering the high sequence similarity within the first three amino acids, the initiation methionine of all cofactor proteins (italics) is most likely post-translationally processed by a bacterial methionine aminopeptidase [38,39]. The amino-terminal glycine cluster is shaded. B-caps, protein B of the sMMO system from *M. capsulatus* (Bath). B-trich, protein B of the sMMO system from *M. trichosporium* OB3b. B-st.M, protein B of the sMMO system from *Methylocystis* sp. strain M. TMOD, protein D of the toluene-4-monooxygenase system from *Pseudomonas mendocina*. T3MO, cofactor protein of the toluene-3-monooxygenase system from *Pseudomonas picketti*. TbmC, cofactor protein of the toluene/benzene-2-monooxygenase system from *Pseudomonas* sp. PH3_ac, cofactor protein from the phenol hydroxylase system from *Acinetobacter calcoaceticus*. P2, cofactor protein P2 from the phenol hydroxylase system from *Pseudomonas putida*. This figure was prepared using the program ALSCRIPT [40].

SDS–PAGE or by amino-terminal sequencing after storage for more than 7 months. This stability was confirmed for several preparations of the triple glycine mutant.

Glycine residues can serve as protein hinges [19], and, by eliminating them, protein conformation is expected to become more rigid. This enhanced rigidity is likely to contribute to the stability of the triple glycine mutant to proteolysis. Moreover, because tertiary structure protects proteins from degradation [20,21], one might conclude that the amino-terminal region is partly flexible and exposed to solvent.

Activity measurements revealed that the full-length G13Q mutant retained full activity, whereas the G10A-G13Q-G16A mutant displayed only about half the catalytic activity of wild-type MMOB (Table 3). The presence of the amino-terminal His_6-tag did not affect activity. By contrast, the amino-terminal d(3-25)B truncation mutant (see below) lacked catalytic activity, consistent with the diminished activity for the natural degradation product d(1-12)B, referred to as B′ [13]. The decreased catalytic activity of the G10A-G13Q-G16A mutant could be related to the reduced flexibility in the amino-terminal hinge region or to steric clashes in MMOH recognition, introduced by the sidechains of the mutated amino acids. The retention of activity in the G13Q mutant is consistent with the fact that homologous B proteins from the *M. trichosporium* OB3b and *Methylocystis* sp. strain M systems contain glutamine in place of glycine at position 13 [16].

The anomalous behavior of full-length MMOB mutants in size exclusion chromatography

To investigate further the role of the amino terminus in determining properties of the protein, we prepared the deletion mutant d(3-25)B, which is analogous to the toluene monooxygenase cofactor protein (Figure 1). Size-exclusion chromatography was performed with the full-length proteins, as well as with the deletion mutant, using a Pharmacia Superdex 75 gel filtration column. Whereas the truncated mutant d(3-25)B ran as expected for its molecular weight (13 kDa), the wild-type MMOB and the

Table 3

Catalytic activities of protein B mutants.

Protein B	Specific activities (nmol min^{-1} mg^{-1})
Wild-type	5091 ± 1143
G13Q	3988 ± 755
G10A-G13Q-G16A	1662 ± 115
His_6-G10A-G13Q-G16A	2284 ± 222
d(3-25)B	0

The catalytic activity of MMOB was determined by monitoring propylene oxide formation during steady-state conditions after adding purified MMOH, MMOR and NADH [37]. d(3-25)B, truncated version of MMOB.

Figure 2

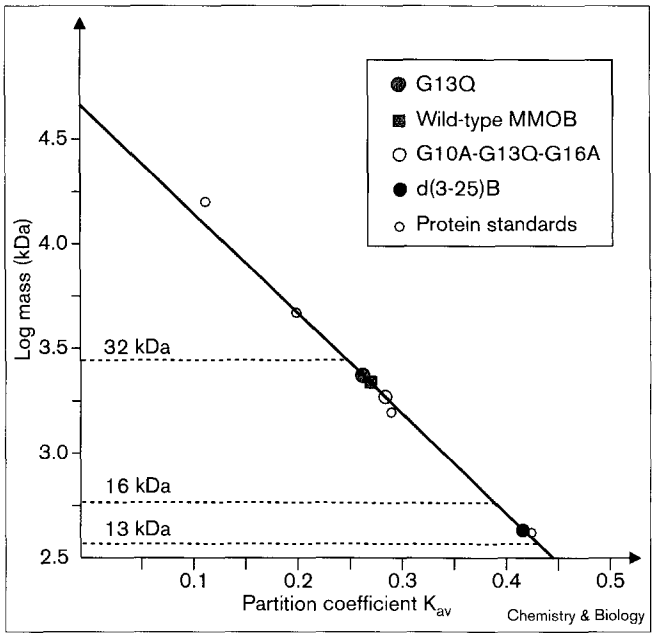

Size exclusion chromatography of protein B mutants. The expected masses for the truncation mutant d(3-25) protein B (13 kDa) and the wild-type and full-length mutants (16 kDa) are indicated by dotted lines.

full-length G13Q and G10A-G13Q-G16A mutants eluted at a retention volume corresponding to molecular weights almost twice their expected values (28 ± 2 kDa; Figure 2). These results suggest either that the amino-terminal segment of MMOB causes dimerization or that it protrudes from the globular fold, projecting into the solvent in such a manner as to reflect an anomalously large apparent size. To investigate the possibility of dimer formation, we carried out multiple gel filtration experiments in the presence of either high salt, 1.5 M NaCl, or detergent, 1.0% Triton-X-100, over a MMOB concentration range from 1–50 mg/ml (0.05–2.5 mM). In each instance we confirmed the previous elution volume; no protein was detected at the elution volume corresponding to a 16 kDa protein as determined by UV absorption spectroscopy and Coomassie-stained SDS gel electrophoresis. The small, but significant, differences in the behavior of wild-type MMOB and the G13Q and G10A-G13Q-G16A mutants on size exclusion columns further support the conclusion that the conformation of the amino-terminal segment is critical for producing the observed retention volumes.

This behavior of MMOB provides valuable structural information. Its anomalous mobility, similar to the tendency of the protein to degrade at the amino terminus, is consistent with the interpretation that the amino-terminal part of polypeptide is unusually flexible, a property enhanced by the cluster of glycine residues Gly10, Gly13 and Gly16.

Figure 3

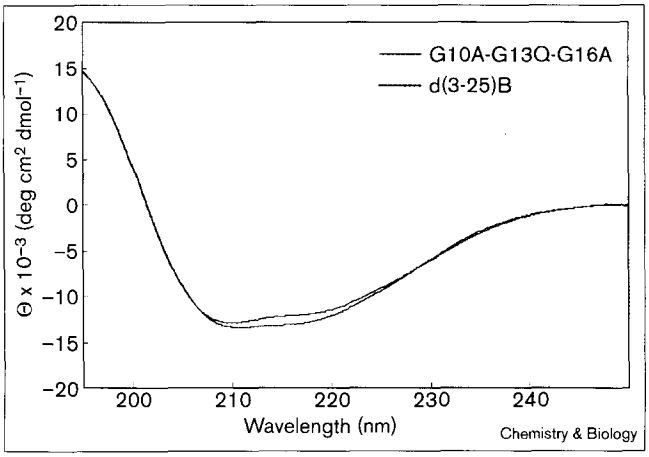

CD spectra of full-length and truncated protein B mutants. The blue spectrum corresponds to the truncation mutant d(3-25)B and the red spectrum to the full-length mutant G10A-G13Q-G16A.

Circular dichroism spectroscopic study of truncated and full-length MMOB mutants

Far-UV circular dichroism (CD) measurements reveal an overall β-folded structure for both the truncated d(3-25)B and full-length G10A-G13Q-G16A MMOB mutants (Figure 3). The CD spectra of the two full-length mutants, G13Q and G10A-G13Q-G16A, are virtually identical (data not shown). The spectrum of the full-length mutant (Figure 3, red) reveals two resolved local ellipticity minima, in contrast to the CD spectrum of d(3-25)B, which does not have a resolved second minimum (Figure 3, blue). In addition, the center of the main minimum of G10A-G13Q-G16A at 209 nm is slightly blue-shifted compared with that of d(3-25)B at 211 nm. The α-helical content therefore is slightly greater in the full-length protein compared with the truncated MMOB mutant d(3-25)B. Conversely, the relative contribution of β sheet appears to be higher in the truncated protein.

The similarity of the CD spectra of the full-length MMOB mutants to the d(3-25)B truncation mutant confirms that the latter indeed forms the folded core of MMOB, consistent with the sequence-alignment analysis (Figure 1). On the basis of the CD data, the secondary structure of this folded core is dominated by β sheets. The slight changes in the CD spectrum of the full-length mutant G10A-G13Q-G16A suggest additional α-helical content.

A three-dimensional structural model for MMOB

The sequence alignment analysis of cofactor proteins related to MMOB (Figure 1) clearly reveals a conserved core with variations in the amino-terminal regions that probably confer specificity for the respective hydroxylase enzymes [22]. The 28% sequence identity between *M. capsulatus* (Bath) MMOB and the P2 cofactor of the

Figure 4

(a) Topological diagram of the protein B model, detailing the sources of information derived from homologous modeling using P2, secondary structure prediction and anomalous sizing behavior. **(b)** Integration of all derived structural information into a three-dimensional ribbon representation of protein B. This figure was generated using the program MOLSCRIPT [41].

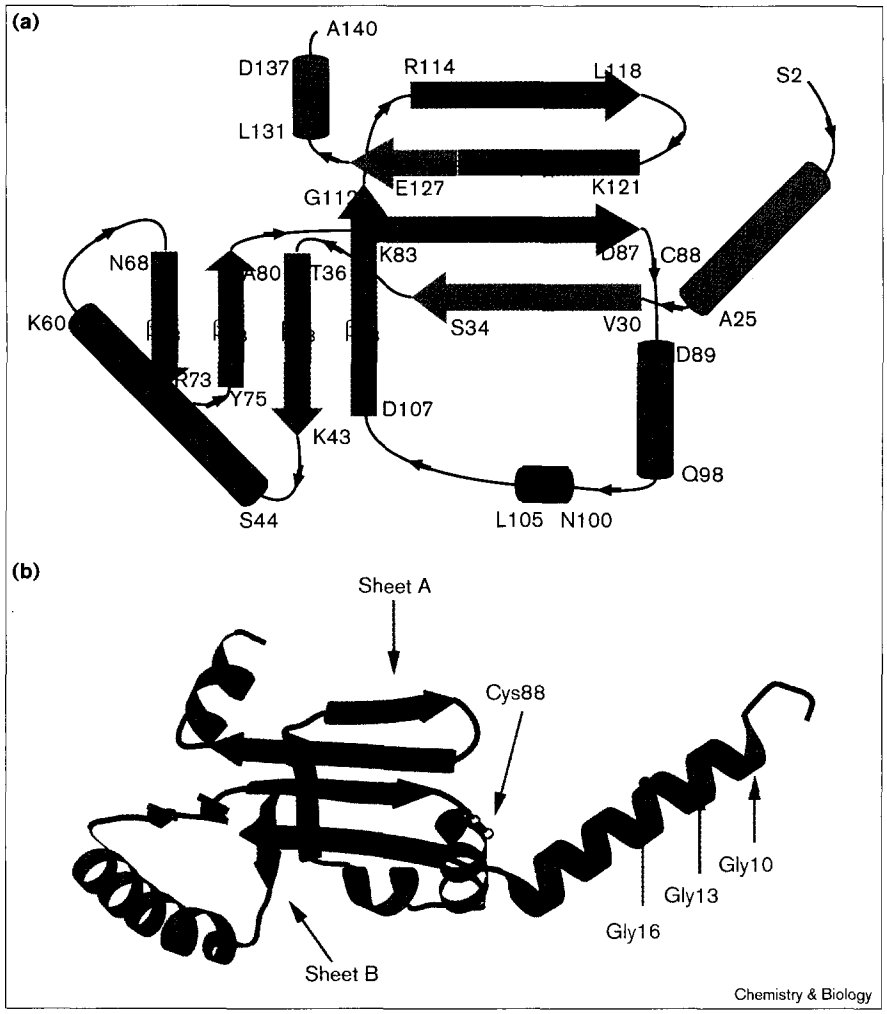

phenol hydroxylase from *P. putida*, for which an NMR structure is available [14], suggests the two proteins share common folding features [23].

In an independent line of investigation, we used reliable secondary structure prediction methods for MMOB [24,25]. In order to cross-check the validity of the two approaches, we first confirmed that the secondary structure elements predicted for MMOB were consistent with the corresponding NMR solution structure of P2. Although the secondary structure derived from P2 is not identical to that of MMOB in every detail, the former provides an unbiased estimate for the latter. The only irreconcilable segment was Asn100–Leu105, which is predicted to adopt an extended conformation but corresponds to a helix in the P2 structure (helix α4, red in Figure 4a). This helical conformation was quite variable within the 12 models comprising the NMR structure ensemble, however (PDB entry code 1hqi) [14]. Two structures (models 2 and 11) adopt a rather distorted backbone geometry in the segment corresponding to helix α4, and fail to exhibit the usual α-helical hydrogen-bonding pattern. For segments where no homologous P2 structure is available (insertions in MMOB compared with P2), the secondary structure prediction algorithms identified three elements (green in Figure 4a). These features are an amino-terminal helix that probably spans Gly10–Ala25 (G16–A25 having highest confidence values, on the basis of the PHD program; α1); a β strand that extends from Val30–Ser34 ($\beta 1_A$); and a short carboxy-terminal helix from Leu131–Asp137 (α5). The secondary structure derived from homology modeling and secondary structure prediction methods, shown in Figure 4a, is fully compatible with the CD data for both the full-length and truncated MMOB mutants (Figure 3).

To model the three-dimensional structure of MMOB, we integrated information obtained from its homology to P2, the predicted secondary structure elements for the sequence insertions, the CD spectroscopic data of the truncated and full-length MMOB mutants, analysis of

Table 4

Probing the accessibility of Cys88 by chemical modification.

	% Protein modification		
Protein B	15 min at 4°C	15 min at 22°C	Unfolded protein
Wild-type MMOB	8	28	100
d(3-25) MMOB	3	26	100

proteolytic fragments, and the gel filtration chromatographic results for the MMOB mutants. We conclude that the polypeptide Asp26–Ala140 folds into a globular core domain, whereas the putative Gly10–Ala25 helix is exposed and protrudes into the solvent. We anticipate, therefore, that strand $\beta1_A$ will be integrated into the core, participating in either antiparallel sheet A or sheet B (Figure 4a), with helix α1 protruding from the resulting compact fold. From the spatial restraints of the P2 structure, strand Val30–Ser34 can extend only sheet A, and not sheet B, in a geometrically sensible way. It was energetically more favorable to allow strand $\beta1_A$ to form hydrogen-bond contacts with strand $\beta2_A$, but the alternative sheet extension with strand $\beta3_A$ could not be excluded. The extension of strand $\beta4_A$ by two amino acids Ser126–Glu127, predicted by the secondary structure algorithm, results in a length matching that of the strand $\beta2_A$ determined in the P2 solution structure. The position of the two helical turns of α5 is restrained by the structural core, but only weakly restricts its precise orientation. The amino-terminal helix α1 is similarly anchored by strand $\beta1_A$, but lacks further intramolecular interactions to stabilize its orientation relative to the protein core. There is a strong crystallographic precedence for the existence of such helical arrangements, including IF3 [26] and pilin [27]. In the case of multicomponent protein systems, similarly exposed helices often serve as intermolecular recognition elements, as exemplified by the α subunit of the G-protein heterotrimer [28].

The ribbon diagram presented in Figure 4b integrates the conclusions from the approaches just delineated into a three-dimensional representation of MMOB. The sole cysteine residue, Cys88, appears to be exposed to the solvent (Figure 4b, blue segment). We attempted, therefore, to test the accessibility of this residue by chemically modifying its thiol group. In the native folded state, Cys88 could be modified only to a limited extent by 5,5′-dithio-bis(2-nitrobenzoic acid) (DTNB) or Ellman's reagent (Table 4), indicating limited accessibility of the residue to the solvent. The truncated d(3-25)B mutant exhibited the same diminished accessibility. These results suggest that Cys88 may be shielded by interactions with the neighboring residues Asn28 or Gln29, but not by the amino-terminal helix α1. In addition, these findings support the strand arrangement in sheet A as depicted in Figure 4 and indicate an affinity of the loop region connecting helix α1 and the first strand $\beta1_A$ for the core of the protein.

Figure 5

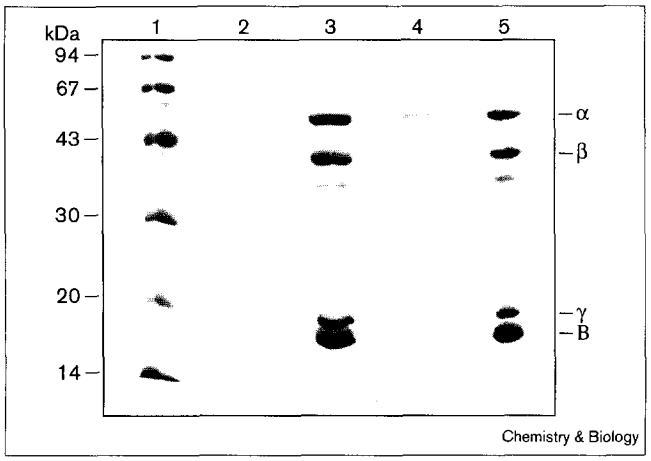

Stabilization of hydroxylase binding to the immobilized protein B column at high ionic strength. Lane 1, molecular weight markers; lane 2, 1 M NaCl wash fraction; lane 3, Ni^{2+} resin after high salt wash; lane 4, 0 M NaCl wash fraction; lane 5 Ni^{2+} resin after no salt wash. At 1 M NaCl, hardly any hydroxylase could be washed off the protein affinity column (lane 2), whereas significantly more hydroxylase is observed in the wash fraction in the absence of salt (lane 4) on a Coomassie stained 13% SDS–PAGE gel.

Proteolytic cleavage of MMOB has been reported to occur between Gln29 and Val30 [13,16]. Neither by amino-terminal sequencing nor by SDS–PAGE could we identify this proteolytic event, not even for G10A-G13Q-G16A samples that were analyzed after more than 7 months storage. This apparent discrepancy might be due to trace amounts of proteases or inhibitors. The reported cleavage site is located before, not within, sheet A and would therefore be consistent with our three-dimensional model of the protein.

Because of its conformational degrees of freedom, we cannot rule out the possibility that the segment of MMOB from Asn5–Met12, located before the free helix α1, could fold back onto the protein core. It was, however, modeled to be exposed to solvent (Figure 4b). It might then function to anchor MMOB to MMOH during complex formation through hydrophobic interactions that are described in more detail below. Such a role would be consistent with the diminished MMOH binding and coupling properties of B′, d(1-12)B [29], and with its lower activity [13]. Experiments with zero-length cross-linking reagents indicate that MMOB binds to the α subunit of MMOH [30]. The E and F helices of the α subunit, exposed in the canyon region of the protein [9], are particularly attractive as a putative binding site for MMOB. In addition to the loop Asn5–Met12, helix Gly10–Ala25 might therefore be involved in helix–helix contacts with the hydroxylase. Both hypotheses can be tested by site-directed mutagenesis, for instance by altering the hydrophilicity of Asn5–Met12 or by introducing a helix-breaking proline residue into the α1 helix.

Since the submission of this paper, two NMR solution structures of MMOB have become available [31,32].

High salt conditions strengthen the binding of the sMMO hydroxylase to MMOB

The His_6-tag enabled us to immobilize reversibly the degradation-resistant triple-glycine MMOB mutant on a Ni^{2+} resin, thereby generating an affinity column for the hydroxylase. The hydroxylase could not be eluted from the mutant MMOB column using high salt (Figure 5, lane 2). In fact, slow elution of the hydroxylase from the MMOB column was significantly higher at low ionic strength than at 1 M NaCl (Figure 5, lane 4). The molar ratio of hydroxylase to MMOB bound to the column after the low salt wash (lane 5) is clearly diminished when compared to that after the high salt wash (lane 3).

Remarkably, in agreement with this behavior, both the hydroxylase and MMOB are very soluble and can be concentrated to >100 mg/ml without precipitating. MMOH–MMOB binding appears to be characterized by a delicately balanced network of interactions that are dominated by hydrophobic contacts. Specific and reciprocal recognition elements are yet to be fully elucidated.

Significance

Protein B (MMOB) serves as an essential cofactor in the soluble methane monooxygenase system of methanotrophic bacteria. We present the first detailed secondary-structural analysis of MMOB. The data are consistent with a prominent amino-terminal α helix that protrudes into the solvent. This feature is related to the proteolytic instability of MMOB and its anomalous size observed in gel-filtration experiments. Using sequence analysis and mutagenesis, we identified a glycine hinge, G10-G13-G16, positioned at the start of the amino-terminal helix. By eliminating this hinge, we generated a catalytically active triple mutant that fully overcomes MMOB degradation. With the amino-terminally His_6-tagged G10A-G13Q-G16A mutant we have demonstrated a way to affinity purify the hydroxylase, facilitating removal of trace contaminants from MMOH. Clearly, the precise functional role of structural elements like the glycine hinge awaits a crystal structure of the MMOH–MMOB complex. To approach this aim, complex crystallization at high ionic strength appears to be a promising approach, given the reverse-phase binding of the hydroxylase and MMOB. Finally, the structural analysis of MMOB presented in this paper provides a rational framework within which further experiments can be planned.

Materials and methods

Cloning enzymes, vectors and bacterial strains

The restriction enzymes *Nde*I and *Xho*I were purchased from New England Biolabs; all others were obtained from Gibco. Proofreading *Vent* polymerase, calf intestinal alkaline phosphatase (CIP), and T4 DNA ligase were purchased from New England Biolabs. 5,5′-Dithio-bis(2-nitro-benzoic acid) (DTNB), Triton X-100, and urea were obtained from Sigma Chemical Company.

The vector pKK223-3 and the *lac* I^q host, *Escherichia coli* strain JM105, were obtained from Pharmacia. The pET-15b vector and the *E. coli* host strain BL21(DE3) were purchased from Novagen. *E. coli* strain XL1-Blue (Stratagene) was used to prepare recombinant plasmids.

The 10 kb plasmid pCH4, which contains the complete *M. capsulatus* (Bath) sMMO operon, was a generous gift from J.C. Murrell (University of Warwick, UK).

Construction of mutant protein B expression vectors

All DNA manipulations were performed according to standard techniques [33]. The cloning of all MMOB mutants was carried out by employing a standard hot start polymerase chain reaction (PCR) protocol, utilizing the proofreading Vent polymerase. Because every MMOB mutant gene has fewer than 450 bases, the complete B construct gene was amplified by PCR using pCH4 as template DNA. The primer sequences were designed by using the Wisconsin Program Package [34]. The forward (fw) and reverse (rv) primers used for the individual mutants are G13Q: fw (60 b) 5′-TGCATT***CATATG***AGCGTAAACAGCAACGCATACGACGCCGGC-ATCATGCAGCTGAAAGGC-3′; rv(33 b) 5′-ATGTCA***CTCGAG***TTACG-CGTGATAGTCTTCGAG-3′. The *Nde*I and *Xho*I restriction sites are bold and italicized. G10A-G13Q-G16A: fw (69 b) 5′-TGCATT***CATATG***AGCG-TAAACAGCAACGCATACGACGCCGCCACATGCAGCTGAAAGCC-AAGGACTTC-3′, with the *Nde*I restriction site bold and italicized. The reverse primer was the same as that used for the G13Q mutant. d(3-25)B: fw (42 b) 5′-GAAACA***GAATTC***ATGAGCGTAGACGAAAACCAAGTG-GTCCAT-3′; rv (54 b) 5′-GTGAT***AAGCTT***ATTA**GTGATGGTGATGGT-GATG**CAGCTCACTAGTAATGGTGAA-3′, with the *Eco*RI and *Hind*III sites bold and italicized and the His_6-tag indicated in bold. This deletion mutant also removes residues 129–140 at the carboxyl terminus of MMOB. After digestion with the respective restriction enzymes, the PCR products were purified using a Qiagen PCR kit. Genes for the G13Q and G10A-G13Q-G16A mutants were inserted into the multiple cloning site of the vector pET15-b, which provides an amino-terminal His_6-tag, using T4 DNA ligase. The gene for truncation mutant d(3-25)B, corresponding to the cofactor of toluene monooxygenase, was cloned into the multiple cloning site of the pKK223-3 vector. To improve efficiency, digested vectors were dephosphorylated with CIP and gel-purified (Qiagen) before ligation. The ligated DNA was transformed into salt-competent XL1-Blue cells. Plasmids containing the desired mutant MMOB genes were identified by restriction digests of DNA isolated from plasmid mini-preparations [33]. All sequences were verified by cDNA sequencing using an Applied Biosystems Model 373 Stretch DNA Sequencer. Competent BL21(DE3) (for G13Q and G10A-G13Q-G16A) or JM105 (for d(3-25)B) cells were transformed with the constructed expression vectors.

Expression and purification of B mutant proteins

The transformed *E. coli* cells, carrying the plasmid coding for the mutants of MMOB, were grown in 1 l quantities of LB ampicillin (100 μg/ml) medium with vigorous shaking at 37°C to an optical density of $A_{600} = 0.6–0.8$. The cultures were then induced with 0.5–0.9 mM isopropyl β-D-thiogalactopyranoside (IPTG) and grown for another 3 h. The cells were harvested by centrifugation, washed with 10 mM Tris pH 8.0, 10 mM β-mercaptoethanol (βME), 100 mM NaCl, and the cell paste was stored at −80°C until used. Cell growth and expression conditions for the JM105 cells, carrying the toluene monooxygenase cofactor analog d(3-25)B, were identical to those of the BL21(DE3) cells. Cells were resuspended in 10 mM Tris pH 8.0, 10 mM βME, 100 mM NaCl, 1 mM EDTA with a standard protease inhibitor mixture present, sonicated and cleared by centrifugation (100,000 × g for 1 h). All protein purification steps were carried out at 4°C. All three mutants carry either an amino-terminal (full-length mutants) or a carboxy-terminal (truncated mutant) His_6-tag. The filtered (0.2 μm) supernatant was therefore applied to 5 ml of a Ni^{2+} resin suspension (Pharmacia) and washed with 50 ml buffer

containing 30 mM imidazole (pH 8.0), 5 mM βME, and 0.5 M NaCl, followed by 50 ml of 30 mM imidazole (pH 8.0), 5 mM βME, 20 mM NaCl. For purification of the His_6-tagged protein, material was eluted from the Ni^{2+} column with 65 mM imidazole (pH 8.0), 5 mM βME, 20 mM NaCl. To remove the His_6-tag, the protein was cleaved with thrombin while still bound to the Ni^{2+} beads. Digestion was carried out overnight at 4°C and stopped by addition of 1 mM phenylmethylsulfonyl fluoride (PMSF, Sigma). As in the wild-type MMOB purification protocol, the protein was then loaded onto a Q-Sepharose column (Pharmacia), washed with 150 mM NaCl, and eluted with a 150–350 mM NaCl gradient. Fractions were pooled based on Coomassie-stained SDS–PAGE analyses. The concentrated sample (Centriprep, Amicon, 10 kDa molecular weight cutoff), was finally loaded onto a Superdex-75 column (Pharmacia), which was equilibrated against the running buffer (25 mM MOPS pH 7.0, 1 mM βME). Protein concentrations were determined from A_{280} by using the extinction coefficient calculated from the amino acid sequence. The concentrated protein (20 mg/ml) was drop-frozen in liquid N_2 and stored at –80°C. From 1 l of cell culture, more than 10 mg of protein was obtained for each mutant with a purity of better than 99% based on SDS–PAGE. To monitor degradation resistance, amino-terminal sequencing was performed using an Applied Biosystems Model 477A Protein Sequencer.

Mass spectrometry

All mutant proteins were confirmed by matrix-assisted laser desorption/ionization time-of-flight (MALDI–TOF) mass spectral analysis using a Perceptive Biosystems Voyager-DE mass analyzer. The spectrometer was operated in positive ion mode at an acceleration potential of 25 kV. The samples, at 1 mM concentration, were mixed with the sinapinic acid matrix and, after air drying for 10 min, washed with 0.1% trifluoroacetic acid. Spectra were calibrated with myoglobin. The determined masses match well with the calculated masses, indicating that all start methionines are cleaved. The calculated masses are listed in parentheses. His_6-G10A-G13Q-G16A 18,107 Da (18,115 Da); G10A-G13Q-G16A (thrombin cleaved) 16,361 Da (16,364 Da); His_6-G13Q 18,089 Da (18,087 Da); G13Q (thrombin cleaved) 16,333 Da (16,336 Da); d(3-25)B 12778 Da (12783 Da).

Size exclusion chromatography

All analytical gel filtration experiments were performed on a Pharmacia fast protein liquid chromatography (FPLC) system using a Pharmacia Superdex 75 HiLoad 16/60 gel filtration column at 4°C. The column was calibrated with the following protein standards: ribonuclease A, 13.7 kDa, chymotrypsinogen A, 25.0 kDa, RuvC, 37.2 kDa, and bovine serum albumin, 66.4 kDa. Based on multiple runs, the retention volume errors are less than 1%. The molecular weights of the calibration proteins were plotted semilogarithmically versus the partition coefficient K_{av} to determine the apparent molecular mass of the sample. K_{av} is defined as the ratio $(V_e-V_0)/(V_t-V_0)$. V_e, V_0 and V_t represent the elution, void and total column volume, respectively [35], with $V_0 = 32$ ml and $V_t = 115$ ml.

Chemical modification of Cys88

Protein concentrations were determined from A_{280} measurements. Samples were prepared in 0.1 M sodium phosphate, pH 8.1. Urea (7 M) was included to produce denatured samples. Protein solutions and cysteine standard solutions were mixed with DTNB by gentle shaking for 15 min. The amount of modified cysteine was then determined spectroscopically by measuring the absorbance at 412 nm. The amount of modified cysteine was quantitated against standard solutions containing known amounts of cysteine and the percent of modification was calculated by reference to the originally determined protein concentration.

Circular dichroism spectroscopy

Protein samples were dialyzed against buffer containing 10 mM Tris pH 7.5, 50 mM NaCl. CD measurements were performed at 4°C on a Jasco Spectropolarimeter J-715 using a 0.1 cm quartz cuvette. To avoid pipetting errors, protein concentrations were determined from A_{280} measurements made on the CD samples. The concentrations were 11.3×10^{-6} M and 7.9×10^{-6} M for d(3-25)B and G10A-G13Q-G16A, respectively. All spectra were baseline corrected by calibration with the dialysis buffer. Spectra were scanned from 250–195 nm at a speed of 50 nm/min, band-width of 1.0 nm, and resolution of 0.1 nm. Ten runs were accumulated and averaged. Noise reduction was performed on the normalized spectra, employing Fourier filtering methods as implemented in the Jasco software. CD measurements are reported as mean residue ellipticity, Θ, in degrees × cm^2 × $dmol^{-1}$.

Sequence alignment, secondary structure prediction and model building

Sequence alignments were calculated by using the program AMPS [22], in which the Dayhoff mutation data matrix was employed to determine multiple alignments. The results for the multiple alignments were robust over a broad range (2.0–15.0) of input gap penalties. By contrast, pairwise sequence alignment calculations were in general not robust, but very much depended on the input parameters. The secondary structure and solvent accessibility were calculated by using the automated PHD algorithm [24,25]. In this method, the neural network employed by the PHD algorithm was trained by a set of high-resolution X-ray protein structures, not including the NMR results for protein P2. The target MMOB sequence was aligned with protein sequences of higher than 30% identity, for which a common protein fold is assumed. The reliability of the predicted secondary structures and solvent accessiblites is weighted by the PHD program based on the agreement within the aligned protein sequences. The three-dimensional model building and subsequent energy refinement were carried out by using the program MAIN [36]. Sidechains of homologous regions of the P2 protein were replaced by the MMOB counterparts, and the few conflicting geometries were manually corrected. The structure was then expanded by applying ideal structural topologies for the inserted segments. This structure was then regularized by energy minimization. In addition to conformational energy terms for bond, angle, and dihedral angle geometries, and a nonbonded van der Waals potential, the energy function included a harmonic energy term which restrained the C_α-positions of the homologous segments to the P2 C_α coordinates with a force constant of 10 kcal/(mol $Å^2$).

Salt dependence of hydroxylase binding to MMOB and enzyme activity assays

All binding studies were performed at 4°C. Growth of *M. capsulatus* (Bath) cells and purification of the hydroxylase component were carried out as described previously [37]. His_6-tagged MMOB mutants were first applied to 1 ml of suspended Ni^{2+} beads and equilibrated for 30 min under continuous gentle shaking. To remove weakly bound MMOB from the Ni^{2+} resin, it was washed with several column volumes of 25 mM MOPS pH 7.0, 1 mM βME, 0.5 M NaCl. The resin was resuspended in 1 ml of the previous washing buffer and gently mixed for 15 min with a total of 1.5 mg of hydroxylase, corresponding to a MMOH to MMOB molar ratio of 1:3. The resin was poured back to the column and then washed with five column volumes of 25 mM MOPS pH 7.0, 1 mM βME, 1 M NaCl buffer. A sample from the column resin was taken for analysis by SDS–PAGE (lane 3, Figure 5). Next, the column was washed with five column volumes of 25 mM MOPS pH 7.0, 1 mM βME, 0 M NaCl buffer. Again a sample was taken from the column resin for analysis (lane 5, Figure 5). Finally, fractions following both the high and low salt washes were loaded onto the SDS–PAGE gel (Figure 5, lane 2 and 4, respectively). Enzymatic activity was monitored by propylene oxide formation, as described previously [37].

Acknowledgements

We thank F. Poy for assistance with mass spectrometry and we thank the members of both laboratories, in particular F. Poy, H.-J. Nam and J. Augustine, for advice and discussion. Protein and DNA sequencing was performed at the Core Facility at the DFCI. H.B. is grateful to the Alexander von Humboldt foundation for a Feodor-Lynen research fellowship; D.A.W. is an NIH Biotechnology predoctoral trainee. This work was supported by grants from the National Institute of General Medical Sciences (GM32134 to S.J.L. and GM48388 to S.J.L. and C.A.F.).

References

1. Starr, C., Searl, M.F. & Alpert, S. (1992). Energy sources: a realistic outlook. *Science* **256**, 981-987.
2. Sullivan, J.P. & Chase, H.A. (1996). 1,2,3-Trichlorobenzene transformation by *Methylosinus trichosporium* OB3b expressing soluble methane monooxygenase. *Appl. Microbiol. Biotechnol.* **45**, 427-433.
3. Jahng, D., Kim, C.S., Hanson, R.S. & Wood, T.K. (1996). Optimization of trichloroethylene degradation using soluble methane monooxygenase of *Methylosinus trichosporium* OB3b expressed in recombinant bacteria. *Biotechnol. Bioeng.* **51**, 349-359.
4. Green, J. & Dalton, H. (1989). Substrate specificity of soluble methane monooxygenase. *J. Biol. Chem.* **264**, 17698-17703.
5. Liu, K.E., Johnson, C.C., Newcomb, M. & Lippard, S.J. (1993). Radical clock substrate probes and kinetic isotope effect studies of the hydroxylation of hydrocarbons by methane monooxygenase. *J. Am. Chem. Soc.* **115**, 939-947.
6. Oremland, R.S. & Culbertson, C.W. (1992). Importance of methane-oxidizing bacteria in the methane budget as revealed by the use of a specific inhibitor. *Nature* **356**, 421-423.
7. Stubbe, J. (1990). Ribonucleotide reductases. *Adv. Enzymol.* **63**, 349-419.
8. Nordlund, P. & Eklund, H. (1995). Diiron-carboxylate proteins. *Curr. Opin. Struct. Biol.* **5**, 758-766.
9. Rosenzweig, A.C., Brandstetter, H., Whittington, D.A., Nordlund, P., Lippard, S.J. & Frederick, C.A. (1997). Crystal structures of the methane monooxygenase hydroxylase from *Methylococcus capsulatus* (Bath): implications for substrate gating and component interactions. *Proteins* **29**, 141-152.
10. Liu, K.E. & Lippard, S.J. (1991). Redox properties of the hydroxylase component of methane monooxygenase from *Methylococcus capsulatus* (Bath). *J. Biol. Chem.* **266**, 12836-12839, 24859.
11. Green, J. & Dalton, H. (1985). Protein B of soluble methane monooxygenase from *Methylococcus capsulatus* (Bath). *J. Biol. Chem.* **260**, 15795-15801.
12. Pilkington, S.J., Salmond, G.P.C., Murrell, J.C., & Dalton, H. (1990). Identification of the gene encoding the regulatory protein B of soluble methane monooxygenase. *FEMS Microbiol. Lett.* **72**, 345-348.
13. Lloyd, J.S., Bhambra, A., Murrell, J.C. & Dalton, H. (1997). Inactivation of the regulatory protein B of soluble methane monooxygenase from *Methylococcus capsulatus* (Bath) by proteolysis can be overcome by a Gly to Gln modification. *Eur. J. Biochem* **248**, 72-79.
14. Qian, H., Edlund, U., Powlowski, J., Shingler, V. & Sethson, I. (1997). Solution structure of phenol hydroxylase protein component P2 determined by NMR spectroscopy. *Biochemistry* **36**, 495-504.
15. Nordlund, I., Powlowski, J. & Shingler, V. (1990). Complete nucleotide sequence and polypeptide analysis of multicomponent phenol hydroxylase from pseudomonas sp. Strain CF600. *J. Bacteriol.* **172**, 6826-6833.
16. Shinohara, Y., Uchiyama, H., Yagi, O. & Kusukabe, I. (1998). Purification and characterization of component B of a soluble methane monooxygenase from *Methylocystis* sp. M. *J. Ferment. Bioeng.* **85**, 37-42.
17. Schechter, I. & Berger, A. (1967). On the size of active site in proteases. I. Papain. *Biochem. Biophys. Res. Commun.* **27**, 157-162.
18. McDonald, I.R., Uchiyama, H., Kambe, S., Yagi, O. & Murrell, J.C. (1997). The soluble methane monooxygenase gene cluster of the trichloroethylene-degrading methanotroph *Methylocystis* sp. strain M. *Appl. Environ. Microbiol.* **63**, 1898-1904.
19. Veltman, O.R., Eijsink, V.G.H., Vriend, G., de Kreij, A., Venema, G., & Van den Burg, B. (1998). Probing catalytic hinge bending motions in thermolysin-like proteases by glycine→alanine mutations. *Biochemistry* **37**, 5305-5311.
20. Zhang, F., Kartner, N. & Lukacs, G.L. (1998). Limited proteolysis as a probe for arrested conformational ,maturation of ΔF508 CFTR. *Nat. Struct. Biol.* **5**, 180-183.
21. Fontana, A., Polverino de Laureto, P., De Filippis, V., Scaramella, E. & Zambonin, M. (1997). Probing the partly folded states of proteins by limited proteolysis. *Fold. Des.* **2**, R17-R26.
22. Barton, G.J. & Sternberg, M.J. (1987). A strategy for the rapid multiple alignment of protein sequences. Confidence levels from tertiary structure comparisons. *J. Mol. Biol.* **198**, 327-337.
23. Russell, R.B., Saqi, M.A.S., Sayle, R.A., Bates, P.A. & Sternberg, M.J.E. (1997). Recognition of analogous and homologous protein folds: analysis of sequence and structure conservation. *J. Mol. Biol.* **269**, 423-439.
24. Rost, B. & Sander, C. (1994). Combining evolutionary information and neural networks to predict protein secondary structure. *Proteins* **19**, 55-72.
25. Rost, B. & Sander, C. (1993). Prediction of protein structure at better than 70% accuracy. *J. Mol. Biol.* **232**, 584-599.
26. Biou, V., Shu, F. & Ramakrishnan, V. (1995). X-ray crystallography shows that translational initiation-factor IF3 consists of two compact α/β domains linked by an α-helix. *EMBO J.* **14**, 4056-4064.
27. Parge, H.E., Forest, K.T., Hickey, M.J., Christensen, D.A., Getzoff, E.D. & Tainer, J.A. (1995). Structure of the fibre-forming protein pilin at 2.6 Å resolution. *Nature* **378**, 32-38.
28. Wall, M.A., *et al.*, & Sprang, S.R. (1995). The structure of the G protein heterotrimer $G_{i\alpha 1}\beta_1\gamma_2$. *Cell* **83**, 1047-1058.
29. Kazlauskaite, J., Hill, H.A.O., Wilkins, P.C. & Dalton, H. (1996). Direct electrochemistry of the hydroxylase of soluble methane monooxygenase from *Methylococcus capsulatus* (Bath). *Eur. J. Biochem.* **241**, 552-556.
30. Fox, B.G., Liu, Y., Dege, J.E., & Lipscomb, J.D. (1991). Complex formation between the protein components of methane monooxygenase from *Methylosinus trichosporium* OB3b. *J. Biol. Chem.* **266**, 540-550.
31. Chang, S.-L., Wallar, B.J., Lipscomb, J.D. & Mayo, K.H. (1999). Solution structure of component B from methane monoxygenase derived through heteronuclear NMR and molecular modeling. *Biochemistry* **38**, 3799-3812.
32. Walters, K.J., Gassner, G.T., Lippard, S.J. & Wagner, G.H. (1999). Structure of the soluble methane monooxygenase regulatory protein B. *Proc. Natl Acad. Sci. USA* **96**, in press.
33. Sambrook, J., Fritsch, E.F., & Maniatis, T. (1989). *Molecular Cloning: A Laboratory Manual* (2nd ed.). Cold Spring Harbor Laboratory Press.
34. Genetics Computer Group (GCG) (1996), Wisconsin Package Version 9.0, Madison, Wisconsin.
35. Creighton, T.E. (1993). *Proteins: Structures and Molecular Properties* (2nd ed.). W.H. Freeman and Co., New York.
36. Turk, D. (1992). Weiterentwicklung eines Programms für Molekülgraphik und Elektronendichte-Manipulation und seine Anwendung auf verschiedene Protein-Strukuraufklärungen [Development of a computer program for molecular graphics and electron density manipulation and its application to various protein structure determinations; PhD thesis]. Technische Universität München.
37. DeWitt, J.G., *et al.*, & Lippard, S.J. (1991). X-ray absorption, Mössbauer and EPR studies of the dinuclear iron center in the hydroxylase component of methane monooxygenase. *J. Am. Chem. Soc.* **113**, 9219-9235.
38. Ben-Bassat, A., Bauer, K., Chang, S.-Y., Myambo, K., Boosman, A. & Chang, S. (1987). Processing of the initiation methionine from proteins: properties of the *Escherichia coli* methionine aminopeptidase and its gene structure. *J. Bacteriol.* **169**, 751-757.
39. Gonzales, T. & Robert-Baudouy, J. (1996). Bacterial aminopeptidases: properties and functions. *FEMS Microbiol. Rev.* **18**, 319-344.
40. Barton, G.J. (1993). ALSCRIPT: a tool to format multiple sequence alignments. *Protein Eng.* **6**, 37-40.
41. Kraulis, P.J. (1991). MOLSCRIPT: a program to produce both detailed and schematic plots of protein structures. *J. Appl. Crystallogr.* **24**, 946-950.

Because *Chemistry & Biology* operates a 'Continuous Publication System' for Research Papers, this paper has been published via the internet before being printed. The paper can be accessed from http://biomednet.com/cbiology/cmb – for further information, see the explanation on the contents pages.